A Modular and Scalable Structure Using Multiparallel-Connected Series-Voltage Compensators for Supply Voltage Regulation

Victor Sui-Pung Cheung, Henry Shu-hung Chung, *Senior Member, IEEE*, and Alan Wai-Lun Lo, *Member, IEEE*

***Abstract*—A modular and scalable voltage-regulation structure for enhancing service continuity and flexibly changing the system power rating is proposed. The methodology is based on paralleling multiple series-voltage compensators, namely multiparallel-connected series-voltage compensator (MSVC), to regulate the load voltage. The output voltage of each compensator is controlled locally by adjusting the phase angle of the output voltage of the inverter in each compensator, while the output current of each compensator is coupled to two adjacent compensators via two coupling transformers. The coupling transformers form a daisy-chained structure. The load current can be shared near-equally among the compensators through the transformer structure. The operating principle, steady-state and transient current-sharing characteristics of the architecture will be discussed and illustrated. A simplified design procedure will be given. A 3-kVA MSVC test bed with three parallel-connected single-phase compensator units has been built and evaluated. The response of the MSVC system with each compensator unit engaged and disengaged momentarily will be investigated. Such structure is applicable for regulating and stabilizing the supply voltage for consumers at the distribution side.**

***Index Terms*—Ac voltage regulation, daisy-chained transformers, dc–ac power conversion, inverters, synchronous series compensator.**

NOMENCLATURE

v_L	Load voltage.
V_L	Steady-state value of v_L.
$\|v_L\|$	RMS value of v_L.
i_L	Load current.
θ	Phase angle between v_L and i_L.
v_r	Output voltage of the *r*th compensator.
V_r	Steady-state value of v_r.
ϕ_r	Phase angle of v_r.
Φ_r	Steady-state value of ϕ_r.
α	Type of load (Inductive: $\alpha = 1$, Capacitive: $\alpha = -1$).
i_r	Current through the *r*th compensator.
I_r	Amplitude of the maximum current through the compensator.
$\|i_r\|$	RMS value of i_r.
$\|i_{r,\max}\|$	Maximum rms value of i_r.
$\hat{i}_r$	Maximum current ripple on the output.
v_x	Output voltage of the MSVC.
$\|v_x\|$	RMS value of v_x.
ϕ_x	Phase angle of v_x.
f	Line frequency.
ω	Angular line frequency ($2\pi f$).
$\omega_{n,r}$	Natural frequency of *r*th compensator.
ξ_r	Damping ratio of *r*th compensator.
τ	Time constant of the integrator.
f_s	Switching frequency of the inverter.
m	Modulation index of the inverter.
B_m	Maximum flux density of the core.
$C_{\mathrm{dc},r}$	Dc-link capacitor of the *r*th compensator.
$C_{q,r}$	Output filter capacitor in the *r*th compensator.
$L_{q,r}$	Output filter inductor in the *r*th compensator.
K_g	Core geometry value.
K_i	Integral gain of the PI controller.
$K_{i,\mathrm{ext}}$	Integral gain of the supervisory controller.
K_L	Case classification (Case I: $K_L = 1$, Case II: $K_L = -1$).
K_m	Gain of the modulator.
K_p	Proportional gain of PI controller.
T_r	*r*th transformer.
$L_{m,r}$	Magnetizing inductance of T_r.
n_{r}	Turns-ratio of T_r.
N	Total number of parallel-connected series voltage compensator.
N_p	Number of turns of the primary winding.
$p_{\mathrm{dc},r}$	Power flow into $C_{\mathrm{dc},r}$.
$P_{\mathrm{dc},r}$	Steady-state value of $p_{\mathrm{dc},r}$.
P_x	Real power.
pf	Load power factor.
Q_x	Reactive power.
S_T	Apparent power.
$v_{\mathrm{dc},r}$	Dc-link capacitor voltage of the *r*th compensator.
$V_{\mathrm{dc},r}$	Steady-state value of $v_{\mathrm{dc},r}$.
$\hat{v}_{\mathrm{dc},r}$	Maximum voltage ripple on $C_{\mathrm{dc},r}$.
$v_{Lq,r}$	Maximum voltage drop across $L_{q,r}$.
$v_{o,r}$	Load voltage of the *r*th compensator.
$V_{o,r}$	Steady-state value of $v_{o,r}$.
$\|v_{o,r}\|$	RMS value of $v_{o,r}$.
$v_{\mathrm{ref},r}$	Reference voltage of the *r*th compensator.
$v_{\mathrm{ref,ext}}$	External reference voltage of the *r*th compensator.
v_s	Ac mains voltage.

Manuscript received March 25, 2015; revised June 20, 2015; accepted August 7, 2015. Date of publication August 17, 2015; date of current version January 7, 2016. This work was supported by a grant from the Research Grants Council of the Hong Kong Special Administrative Region, China, under Project CityU 112512. Recommended for publication by Associate Editor S. K. Mazumder.

V. S.-P. Cheung and H. S.-h. Chung are with the Centre for Smart Energy Conversion and Utilization Research, City University of Hong Kong, Hong Kong (e-mail: spcheung@cityu.edu.hk; eeshc@cityu.edu.hk).

A. W.-L. Lo is with the Department of Computer Science, Chu Hai College of Higher Education Hong Kong (e-mail: wllo@chuhai.edu.hk).

Color versions of one or more of the figures in this paper are available online at http://ieeexplore.ieee.org.

Digital Object Identifier 10.1109/TPEL.2015.2469156

$\lvert v_s \rvert$	RMS value of v_s.
$v_{T,r}$	Voltage across rth transformer T_r.
$\lvert v_{T,\max} \rvert$	Maximum rms value of $v_{T,r}$.
$\lvert Z_L \rvert$	Magnitude value of load impedance.

I. Introduction

An emerging trend in the electricity industry is a paradigm shift from large power plant to small distributed generation (DG) systems located at the point of consumption. Such architecture has the merits of optimizing the asset utilization and power quality, and system reliability, flexibility, and capacity [1], [2]. It operates like the centralized power systems except that the system coverage and operation are being down scaled and are based on a high degree of automated functions. It is thus crucial to provide the loads with a regulated supply voltage.

Traditional voltage regulation method can be categorized into two main approaches: transformer-based regulators and inverter-based voltage regulators. The transformer-based regulators regulate the voltage by using mechanical devices to select appropriate position of the taps on a transformer or of the movable contacts on an autotransformer [3]–[5]. However, the dynamic response of the entire system is limited by the slow movement of the taps or movable contacts. The maintenance cost is also high. The inverter-based regulators make use of power electronics technology to regulate the output voltage. The idea is based on first rectifying the incoming ac voltage into a dc voltage and then converting it back to an ac voltage. Such architecture is suitable for applications requiring variable voltage and variable frequency output, such as motor drives [6]–[8]. As the entire system consists of two power conversion stages, the energy efficiency would sometimes give challenges to designers in managing heat dissipation and increasing the power density. Since the regulator has to process total load power, the Volt-Ampere (VA) rating of the regulator has to be equal to or larger than the maximum rating of the whole system. Thus, the required size, weight, and cost introduce additional design constraints.

Series voltage compensator (SVC), which consists of a voltage source inverter connected in series between the ac mains and the load, is a simple solution for load-voltage restoration and regulation [9]–[14] with the output frequency the same as the frequency of the ac mains. The main advantage is that the required VA rating is smaller than the rating of the entire system as the SVC only compensates the difference between the ac mains voltage and load voltage.

A straightforward approach to meeting the required power rating is the use of a single unit. However, the power ratings of the loads in DG systems are of wide diversity. Thus, a modular and scalable approach is preferred. The efficient way to enhance modularity and scalability is to use multiple units of regulators in parallel to form a modular-based architecture. This can also help the stock management. The main challenge of paralleling multiple regulators is to ensure the current flow through each unit does not exceed the maximum current in both steady state and transient. Conventional current-sharing approaches are based on master-slave control [15]–[18], centralized control [19]–[21], and average load sharing [22]–[24]. These control methods regulate the output voltage and, at the same time, control the current sharing by using multiple control loops, giving challenges to designers about the system stability and control mechanism. Those methods highly rely on the intercommunication line among units. Thus, the system reliability and modularity are the major concerns in the system design. Most importantly, if one/some of the units fail(s), the operation of the rest of the units might be affected.

A series voltage regulator using modular-based SVC architecture is proposed. The method enhances the modularity, scalability, adaptability, and service continuity of the voltage regulation system. The concept is based on connecting multiple units of low-power SVC in parallel to form a multiparallel-connected SVC (MSVC) architecture. Each unit is coupled to one another through a coupling transformer and all coupling transformers are daisy chained. The load current is shared among each unit equally during both steady state and transient periods without any external current control. Even if one of the SVCs malfunctions, the rest of the units will not be overloaded and the voltage regulation can still be maintained. Such modular approach allows consumers on the demand side to flexibly optimize and manage the utilization of regulators and manufacturers to produce standardized low-power units for voltage regulation. It also allows hot-swapping without significant interruption to the operation of system. This paper will discuss the modeling and analysis of each unit and the entire MSVC structure. The theoretical predictions will be confirmed experimentally on a 3-kVA test bed.

II. Operating Principles and Analysis of the MSVC Architecture

A voltage regulation system with SVC is presented in this section. It is shown in Fig. 1. The output voltage v_x, which is in phase quadrature with the load current i_L, either leading or lagging, is injected between ac mains v_s and loads. The magnitude of the load voltage v_L is regulated by controlling v_x. By applying the Kirchhoff's voltage law

$$v_s = v_x + v_L. \tag{1}$$

The real power P_x and the reactive power Q_x handled by the MSVC are

$$P_x = \frac{|v_x||v_s|}{|Z_L|}\cos(\phi_x+\theta) - \frac{|v_x|^2}{|Z_L|}\cos\theta \tag{2}$$

$$Q_x = \frac{|v_x||v_s|}{|Z_L|}\sin(\phi_x+\theta) - \frac{|v_x|^2}{|Z_L|}\sin\theta \tag{3}$$

where $|v_s|$ is the rms value of v_s, $|v_x|$ is the rms value of v_x, $|Z_L|$ is the magnitude value of load impedance, ϕ_x is the phase angle of v_x and θ is the angle between v_L and i_L.

Derivations of (2) and (3) are given in the Appendix.

Ideally, $P_x = 0$. However, the practical value of P_x is slightly larger than zero as some energy will be consumed by the

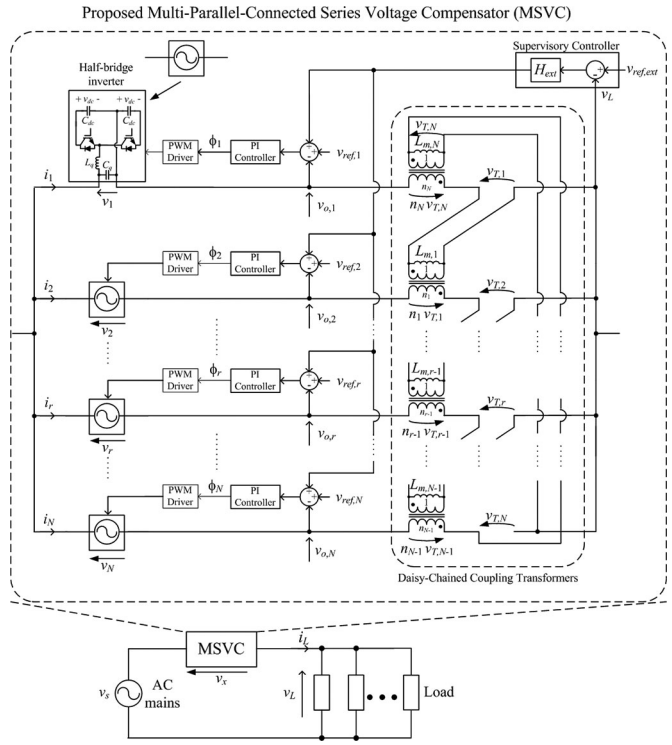

Fig. 1. Schematic of MSVC.

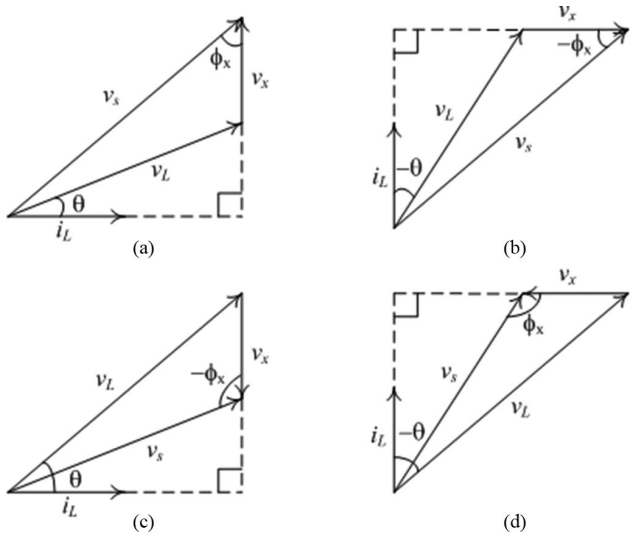

Fig. 2. Four possible operating scenarios in Case I ($|v_L| < |v_s|$) and Case II ($|v_L| > |v_s|$).

compensators in the MSVC. There are in total four possible operational scenarios under inductive and capacitive load, respectively. The phasor diagrams of the scenarios are illustrated in Fig. 2. They are classified into two cases: Case I and Case II. In Case I, $|v_L| < |v_s|$, where $|v_L|$ is the rms value of v_L. In Case II, $|v_L| > |v_s|$. It can be shown that

$$|v_x| = K_L[\sqrt{|v_s|^2 - (|v_L|\cos\theta)^2} - |v_L|\sin(\alpha\theta)] \quad (4)$$

$$\phi_x = K_L \alpha \sin^{-1}\left(\frac{|v_L|}{|v_s|}\cos\theta\right) \quad (5)$$

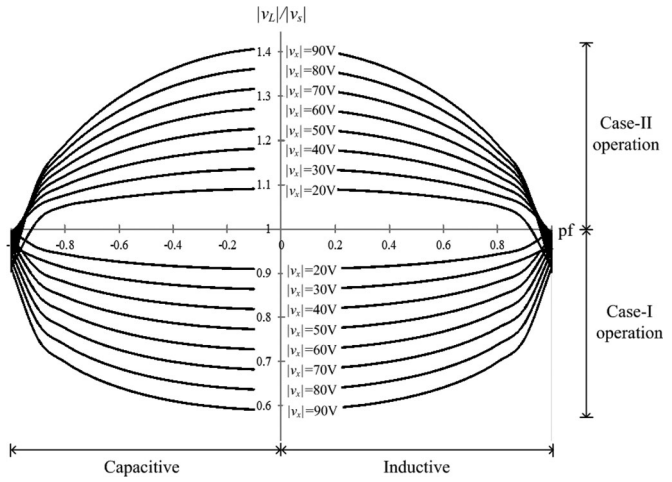

Fig. 3. $|v_L|$ versus power factor (pf) and $|v_x|$.

where $K_L = 1$ for Case I and $K_L = -1$ for Case II, $\alpha = 1$ for inductive load and $\alpha = -1$ for capacitive load.

Derivations of (4) and (5) are given in the Appendix.

Based on (4), Fig. 3 shows the relationships between $|v_L|/|v_s|$ and load power factor (pf), $\cos\theta$, under a given magnitude of v_x. Thus, the controller has to take the load type and the operating case into account to adjust ϕ_x for regulating v_L.

Instead of using one SVC, an architecture that consists of *N* parallel-connected series voltage compensator (MSVC) is proposed. It is shown in Fig. 1. The MSVC is connected in series between ac mains v_s and loads. The load current i_L is shared among the compensators through transformers $T_1, T_2 \ldots, T_N$, which are connected in the form of a daisy-chain [25]. The primary and secondary sides of each transformer are connected to two adjacent compensators, so that the currents through the two connected compensators are in a ratio determined by the ratio between the number of turns on the primary side and the secondary side. The proposed modular-based architecture allows the power rating of the entire regulator system to become scalable. Modeling of the single phase system with the proposed MSVC architecture, and individual compensator unit are studied as follows.

A. Modeling of MSVC

Consider a generic branch *r*. If the voltage across the MSVC configuration is v_x

$$-n_{r-1}v_{T,r-1} + v_{T,r} + v_r = v_x, \text{for } r = 1, 2, \ldots, N, n_0 = n_N \text{ and } v_{T,0} = v_{T,N} \quad (6)$$

where n_{r-1} is the turns-ratio of the transformer T_{r-1}, $v_{T,r}$ is the voltage across the transformer T_r, and v_r is the voltage generated by the *r*th compensator.

Let $v = [v_1\ v_2\ \ldots\ v_r\ \ldots\ v_N]^T$ and $v_T = [v_{T,1}\ v_{T,2}\ \ldots\ v_{T,r}\ \ldots\ v_{T,N}]^T$. The following matrix equation can be formulated by expanding (6):

$$v + Kv_T = \beta v_x \quad (7)$$

where

$$K = \begin{bmatrix} 1 & 0 & & \cdots & & 0 & -n_N \\ -n_1 & 1 & 0 & & \cdots & & 0 \\ 0 & -n_2 & 1 & 0 & & \cdots & \\ & 0 & \ddots & \ddots & \ddots & & \vdots \\ \vdots & \cdots & \ddots & -n_r & \ddots & \ddots & \\ & \cdots & & \ddots & \ddots & 1 & 0 \\ 0 & & \cdots & & 0 & -n_{N-1} & 1 \end{bmatrix} \text{ and}$$

$$\beta = \begin{bmatrix} 1 \\ 1 \\ \vdots \\ 1 \\ 1 \end{bmatrix}.$$

Consider the transformer T_r

$$\begin{aligned} v_{T,r} &= (i_r - n_r i_{r+1}) s L_{m,r}, \text{ for } r \\ &= 1, 2, \ldots, N, \text{ and } n_{N+1} = n_1 \end{aligned} \tag{8}$$

where i_r is the current of the *r*th compensator and $L_{m,r}$ is the magnetizing inductance of T_r.

Let $i = [\, i_1 \; i_2 \; \ldots \; i_r \; \ldots \; i_N \,]^T$. The following matrix equation can be formulated by expanding (8):

$$v_T = Z\, i \tag{9}$$

where

$$Z = \begin{bmatrix} sL_{m,1} & -n_1 sL_{m,1} & 0 & \cdots & \cdots & 0 \\ 0 & sL_{m,2} & -n_2 sL_{m,2} & 0 & & \\ & 0 & \ddots & \ddots & & \\ \vdots & & \ddots & sL_{m,r} & & \\ & & \cdots & \ddots & & \\ 0 & & & & & \\ -n_N sL_{m,N} & 0 & & & \cdots & \end{bmatrix}$$

$$\begin{bmatrix} \cdots & & 0 \\ & \cdots & \\ \ddots & \cdots & \vdots \\ -n_r sL_{m,r} & \ddots & \\ \ddots & \ddots & 0 \\ & \ddots & -n_{N-1} sL_{m,N-1} \\ \cdots & 0 & sL_{m,N} \end{bmatrix}.$$

Thus, by substituting (9) into (7)

$$KZi = \beta v_x - v. \tag{10}$$

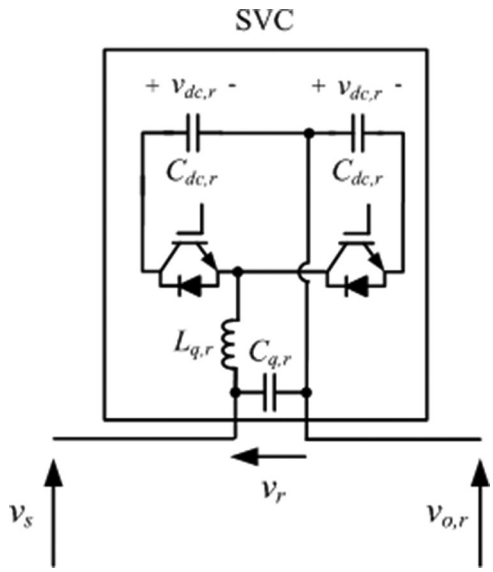

Fig. 4. Circuit schematic of the *r*th compensator.

By applying the Kirchhoff's voltage law for the regulator system

$$v_x = v_s - v_L. \tag{11}$$

By substituting $v_L = i_L Z_L$ into (11)

$$v_x = v_s - i_L Z_L \tag{12}$$

where $i_L = \beta^T i$, in which β^T is the transpose of β.

Substitute (12) into (10)

$$i = Y(\beta v_s - v) \tag{13}$$

where $Y = [KZ + Z_L\{1\}]^{-1}$, and $\{1\}$ is unity matrix.

It should be noted that the steady state of i_r is ideally in phase quadrature with v_r.

By considering the small-signal variations around the operating point in *v* and *i*, the small-signal terms in (13) can be expressed as

$$\Delta i(s) = -Y \Delta v(s) \tag{14}$$

where $\Delta i(s) = [\, \Delta i_1(s) \ldots \Delta i_r(s) \ldots \Delta i_N(s) \,]^T$ and $\Delta v(s) = [\, \Delta v_1(s) \ldots \Delta v_r(s) \ldots \Delta v_N(s) \,]^T$ are the small-signal variations in *i* and *v*, respectively.

(14) is the describing function that describes the small-signal response of the compensator's output currents to the variations in the compensator's output voltages.

B. Modeling of an SVC Unit

Fig. 4 shows the circuit schematic of *r*th compensator unit. The power stage of the compensator is an inverter with its dc side connected to a capacitor $C_{\mathrm{dc},r}$ and its ac side connected in series between the ac mains and the load. The inverter consists of a half-bridge circuit and an output filter formed by the inductor $L_{q,r}$ and capacitor $C_{q,r}$. Without loss of generality, it can be implemented with a full-bridge circuit. The output of the inverter

is v_r, which is in phase quadrature with the branch current i_r, either leading or lagging. The controller senses the load voltage $v_{o,r}$ first and then controls the phase angle ϕ_r of v_r to regulate $v_{o,r}$.

On the dc side of the inverter, the power $p_{\mathrm{dc},r}$ flows into the dc-link capacitor $C_{\mathrm{dc},r}$ is

$$p_{\mathrm{dc},r} = C_{\mathrm{dc},r} v_{\mathrm{dc},r} \frac{dv_{\mathrm{dc},r}}{dt} \tag{15}$$

where $v_{\mathrm{dc},r}$ is dc-link capacitor voltage.

By introducing small-signal perturbations into $p_{\mathrm{dc},r}$ and$v_{\mathrm{dc},r}$

$$p_{\mathrm{dc},r} = P_{\mathrm{dc},r} + \Delta p_{\mathrm{dc},r}(t) \tag{16}$$

$$v_{\mathrm{dc},r} = V_{\mathrm{dc},r} + \Delta v_{\mathrm{dc},r}(t) \tag{17}$$

where $P_{\mathrm{dc},r}$ and $V_{\mathrm{dc},r}$ are the steady-state values of $p_{\mathrm{dc},r}$ and $v_{\mathrm{dc},r}$, respectively.

By putting (16) and (17) into (15)

$$\Delta p_{\mathrm{dc},r} = C_{\mathrm{dc},r} v_{\mathrm{dc},r} \frac{d\Delta v_{\mathrm{dc},r}}{dt}. \tag{18}$$

On the ac side of the inverter, the power flow into the voltage regulator is expressed in (2). By introducing small-signal perturbations into p_r, v_r and ϕ_r, that is

$$p_r(t) = P_r + \Delta p_r(t) \tag{19}$$

$$v_r = V_r + \Delta v_r(t) \tag{20}$$

$$\phi_r = \Phi_r + \Delta\phi_r(t) \tag{21}$$

where V_r and Φ_r are the steady-state values of v_r and ϕ_r, respectively.

By putting (19)–(21) into (2)

$$\Delta p_r(t) = \left[\frac{|v_s||i_r|}{|v_{o,r}|}\cos(\Phi_r+\theta) - \frac{2|v_r||i_r|}{|v_{o,r}|}\cos\theta\right]\Delta v_x(t) - \frac{|v_r||v_s||i_r|}{|v_{o,r}|}\sin(\Phi_r+\theta)\Delta\phi_r(t) \tag{22}$$

where $|i_r|$ is the rms value of i_r and $|v_{o,r}|$is the rms value of $v_{o,r}$.

Based on the law of conservation of energy

$$2\Delta p_{dc}(t) = \Delta p_q(t). \tag{23}$$

By substituting (18) and (22) into (23)

$$4C_{\mathrm{dc},r}\frac{1}{m^2}\frac{d\Delta v_r(t)}{dt} = -\frac{|i_r|}{|v_{o,r}|}\cos\theta_r\Delta v_r(t) - \frac{|v_s||i_r|}{|v_{o,r}|}\sin(\Phi_r+\theta_r)\Delta\phi_r(t) \tag{24}$$

where *m* is the modulation index of the inverter.

After rearranging (24) and taking Laplace transformation

$$G_{1,r}(s) = \frac{\Delta v_r(s)}{\Delta\phi_r(s)} = -\frac{m^2|i_r|(|v_{o,r}| + \alpha|v_r|\sin\theta_r)}{s4C_{dc,r}|v_{o,r}| + |i_r|\cos\theta_r}. \tag{25}$$

The relationship between $v_{o,r}$ and v_r can be found by using the cosine law as

$$|v_{o,r}|^2 = |v_s|^2 + |v_r|^2 - 2|v_s||v_r|\cos\phi_r. \tag{26}$$

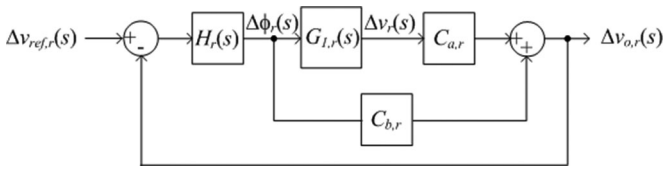

Fig. 5. Small-signal control block diagram of the compensator.

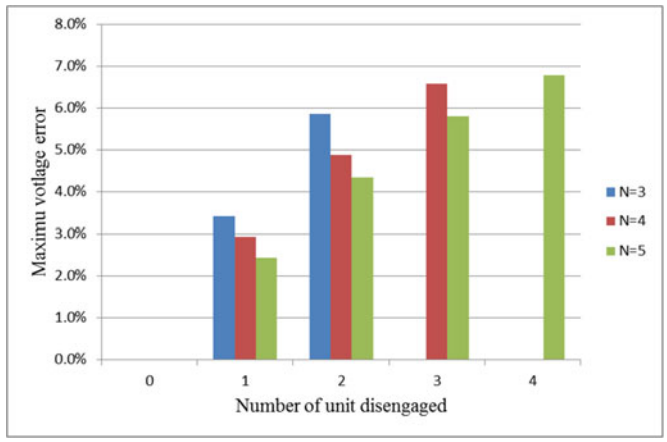

Fig. 6. Maximum steady-state error of v_L versus the number of disengaged unit.

By introducing small-signal perturbations into $v_{o,r}$

$$v_{o,r} = V_{o,r} + \Delta v_{o,r}(t) \tag{27}$$

where $V_{o,r}$ is the steady-state value of $v_{o,r}$.

By substituting (20), (21), and (27) into (26), the small-signal variations around the operating point can be expressed as

$$G_{2,r}(s) = \frac{\Delta v_{o,r}(s)}{\Delta\phi_r(s)} = G_{1,r}(s)C_{a,r} + C_{b,r} \tag{28}$$

where $C_{a,r} = -\sin(\alpha\theta_r)$ and $C_{b,r} = \alpha|v_r|\cos\theta_r$.

A proportional-plus-integral (PI) controller $H_r(s)$ is used to regulate $v_{o,r}$ at the reference voltage $v_{\mathrm{ref},r}$ by altering the angle ϕ_r in each compensator. Fig. 5 shows the small-signal control block diagram of *r*th compensator unit. The closed-loop transfer function $T_{\mathrm{CL},r}(s)$ of voltage regulator is

$$T_{\mathrm{CL},r}(s) = \frac{\Delta v_{o,r}(s)}{\Delta v_{\mathrm{ref},r}(s)} = \frac{H_r(s)G_{2,r}(s)}{1 + H_r(s)G_{2,r}(s)} \tag{29}$$

where $H_r(s) = \alpha K_m(K_p + \frac{K_i}{s})$, in which K_p and K_i are the proportional gain and the integral gain of $H_r(s)$, respectively, and $K_m = \frac{\pi}{180}$ is the gain of the modulator.

Thus, the characteristic equation of $T_{\mathrm{CL},r}(s)$ is

$$s^2 + 2\xi_r\omega_{n,r}s + \omega_{n,r}^2 = 0 \tag{30}$$

where

$$\omega_{n,r} = \sqrt{\frac{\gamma_r K_m K_i|i_r|}{4C_{\mathrm{dc},r}|v_{o,r}|(1 + K_m K_p|v_r|\cos\theta_r)}}$$

TABLE I
COMPONENT VALUES USED IN THE ANALYSIS

Parameter	Value	Parameter	Value
$\|v_s\|$	220 V	f	50 Hz
$\|v_L\|$	205 V	pf	0.85
I_r	10 A	$C_{\mathrm{dc},r}$	3 mF
K_i	10	$C_{q,r}$	13 μF
K_p	1	$L_{q,r}$	0.5 mH
$K_{i,\mathrm{ext}}$	1	$L_{m,r}$	0.2 H
		m	1

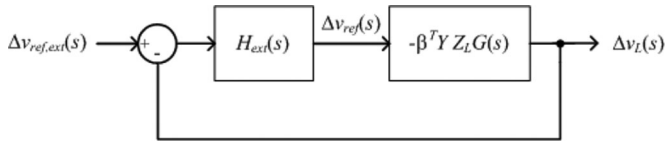

Fig. 7. Small-signal control block diagram of the whole system.

TABLE II
PARAMETER VALUES USED IN MONTE-CARLO SIMULATION

Parameter	Value		
	Min.	Nom.	Max.
$\|\nu_o\|$	198 V	220 V	242 V
pf	$\pm$0.7	0.85	1
$\|\nu_s\|$	220 V		265 V
C_{dc}	2.4 mF	3.0 mF	3.6 mF

is the natural frequency,

$$\xi_r = \frac{4C_{\mathrm{dc}}K_m K_i|v_{o,r}||v_r|\cos\theta_r + \gamma_r K_m K_p|i_r| + |i_r|\cos\theta_r}{8C_{\mathrm{dc}}|v_{o,r}|(1+K_m K_p|v_r|\cos\theta_r)\omega_{n,r}}$$

is the damping ratio, in which $\gamma_r = [\cos^2\theta_r|v_r| + m^2\sin^2\theta_r|v_r| + m^2|v_{o,r}|\sin(\alpha\theta_r)]$.

The poles of $T_{\mathrm{CL},r}(s)$ are

$$s_1, s_2 = -\xi_r\omega_{n,r} \pm j\sqrt{(1-\xi^2)}. \tag{31}$$

(31) shows that all closed-loop poles lie in the left half s-plane.

C. Modeling of the Overall System

The load voltage v_L can be expressed as

$$v_L = \beta^T i\, Z_L. \tag{32}$$

By substituting (13) into (32)

$$v_L = \beta^T Y(\beta v_s - v)Z_L \tag{33}$$

and considering the small-signal variations around the operating point, the small-signal characteristics can be expressed as

$$\Delta v_L(s) = -\beta^T Y\ Z_L\Delta v(s). \tag{34}$$

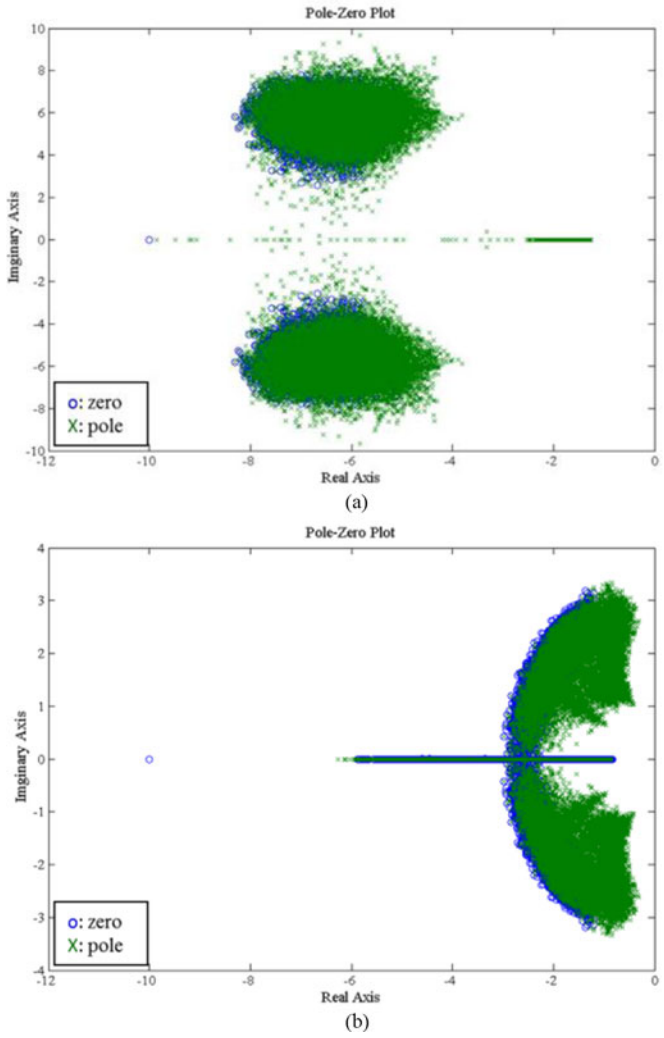

Fig. 8. Pole and zero locations with three units in operation. (a) Full load. (b) 10% load.

Based on (25), (29) and Fig. 5, $\Delta v(s)$can be expressed as

$$\Delta v(s) = G(s)\ \Delta v_{\mathrm{ref}}(s) \tag{35}$$

where $\Delta v_{\mathrm{ref}}(s) = [\,\Delta v_{\mathrm{ref},1} \quad \cdots \quad \Delta v_{\mathrm{ref},r} \quad \cdots \quad \Delta v_{\mathrm{ref},N}\,]^T$ and

$$G(s) = \begin{bmatrix} \left\{\begin{matrix} H_1(s)G_{1,1}(s) \\ [1-T_{\mathrm{CL},1}(s)] \end{matrix}\right\} & 0 & & \\ 0 & \left\{\begin{matrix} H_2(s)G_{1,2}(s) \\ [1-T_{\mathrm{CL},2}(s)] \end{matrix}\right\} & 0 & \\ & \ddots & \ddots & \\ \vdots & & 0 & \\ 0 & & \cdots & \end{bmatrix}$$

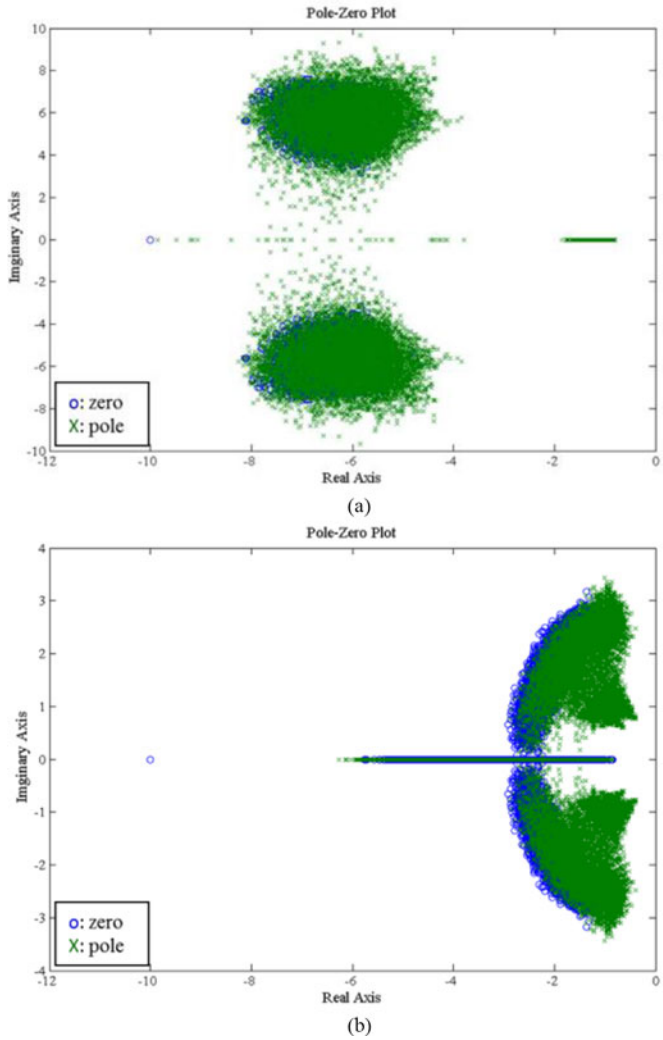

Fig. 9. Pole and zero locations with two units in operation. (a) Full load. (b) 10% load.

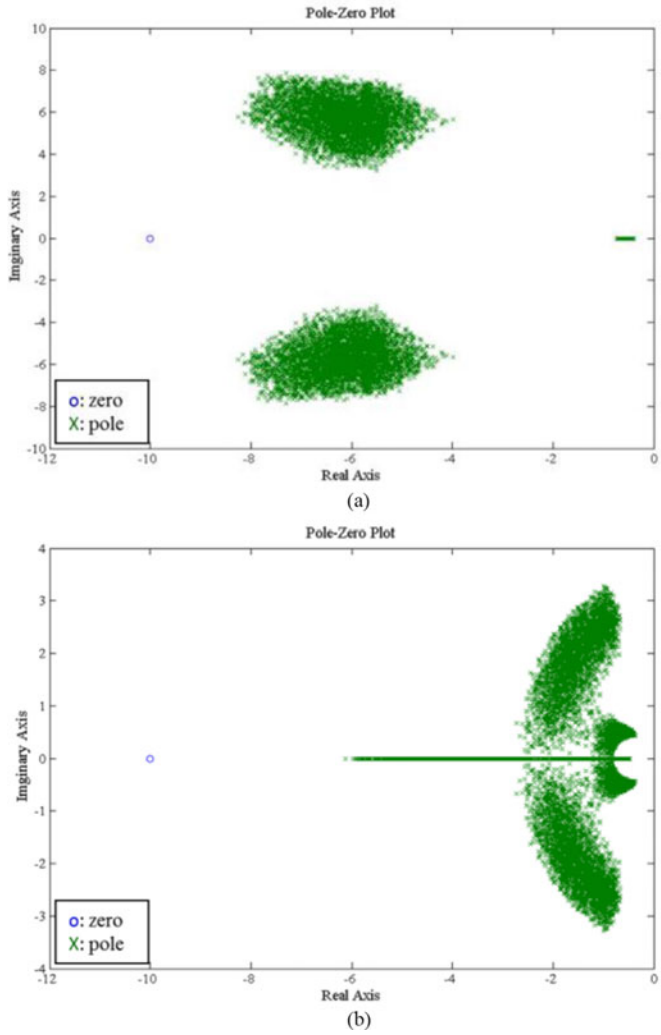

Fig. 10. Pole and zero locations with one unit in operation. (a) Full load. (b) 10% load.

$$\begin{bmatrix} \cdots & & 0 \\ \ddots & & \vdots \\ \left\{ \begin{matrix} H_r(s)G_{1,r}(s) \\ [1-T_{\mathrm{CL},r}(s)] \end{matrix} \right\} & 0 & \\ \ddots & \ddots & 0 \\ & 0 & \left\{ \begin{matrix} H_N(s)G_{1,n}(s) \\ [1-T_{\mathrm{CL},N}(s)] \end{matrix} \right\} \end{bmatrix}.$$

By substituting (35) into (34), the variations of the load voltage Δv_L can be expressed as

$$\Delta v_L(s) = -\beta^T\ Y\ Z_L\ G(s)\ \Delta v_{\mathrm{ref}}(s). \tag{36}$$

Assuming that all coupling transformers are identical, (36) can be expanded into

$$\begin{aligned} \Delta v_L(s) = & -\frac{1}{N}H_1(s)G_{1,1}(s)[1-T_{\mathrm{CL},1}(s)]\Delta v_{\mathrm{ref},1}(s) - \ldots \\ & -\frac{1}{N}H_r(s)G_{1,r}(s)[1-T_{\mathrm{CL},r}(s)]\Delta v_{\mathrm{ref},r}(s) - \ldots \\ & -\frac{1}{N}H_N(s)G_{1,N}(s)[1-T_{\mathrm{CL},N}(s)]\Delta v_{\mathrm{ref},N}(s) \end{aligned} \tag{37}$$

in which they have the common denominator of

$$s^2 + 2\xi_r\omega_{n,r}s + \omega_{n,r}^2. \tag{38}$$

Based on (31) and (38), the closed-loop poles of the overall system lie in the left half s-plane, confirming the stability of the MSVC.

For the sake of simplicity, the steady-state error of v_L is obtained by using numerical method based on (33). Fig. 6 shows the maximum steady-state error of v_L in terms of the number of units disengaged for N varying from three to five. The component values used in the analysis are shown in Table I. It can be shown that the error equals zero if all units operate normally.

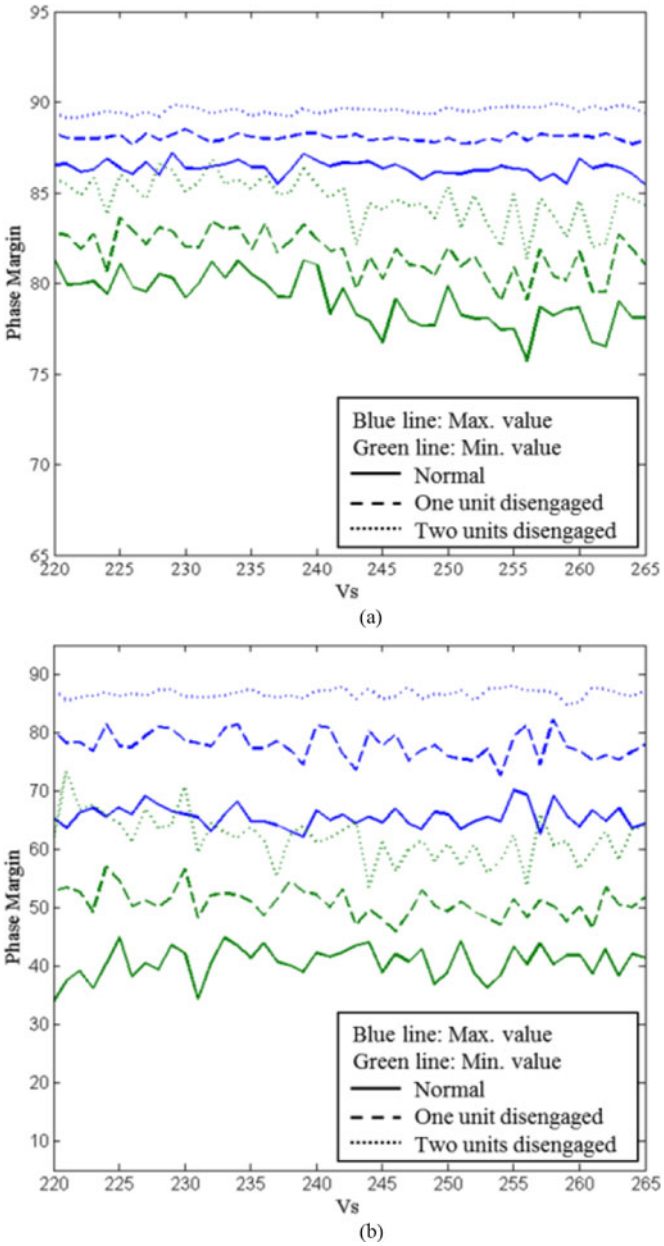

Fig. 11. Phase margin versus $|\nu_s|$. (a) Full load. (b) 10% load.

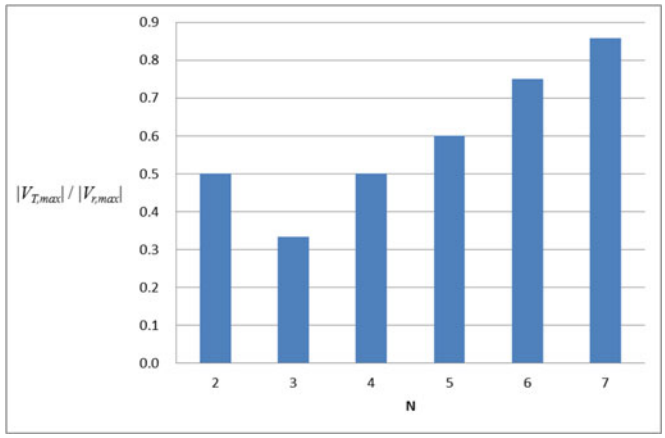

Fig. 12. $|v_{T,\max}|$ versus *N*.

TABLE III
DESIGN SPECIFICATIONS

Parameter	Value	Parameter	Value
f_s	20 kHz	m	1
I_r	10 A	$\hat{v}_{\mathrm{dc},r}$	2 V
$\hat{i}_r$	1 A	$v_{Lq,r}$	2 V

However, if one of the units malfunctions or is disengaged, an error caused by the output voltage difference among each unit occurs. Therefore, a supervisory controller $H_{\mathrm{ext}}(s)$ is added to reduce the error of v_L by adjusting the setting point of v_{ref} in each unit. The implementation is shown in Fig. 1. The controller first senses and compares the load voltage with the external reference, $v_{\mathrm{ref,ext}}$, which is the expected load voltage. Then the controller generates a reference signal based on the voltage difference to offset v_{ref} in each unit. Fig. 7 shows the control block diagram of the whole system.

Based on Fig. 7, the load voltage v_L can be expressed as

$$\Delta v_L = -\beta^T\ Y\ Z_L\ G(s)\ H_{\mathrm{ext}}(s)[\Delta v_{\mathrm{ref,ext}}(s) - \Delta v_L(s)] \tag{39}$$

where $H_{\mathrm{ext}}(s) = K_{i,\mathrm{ext}}/s$, in which $K_{i,\mathrm{ext}}$ is the integral gain of $H_{\mathrm{ext}}(s)$.

The overall transfer function is

$$\frac{\Delta v_L(s)}{\Delta v_{\mathrm{ref,ext}}(s)} = \frac{-\beta^T\ Y\ Z_L\ G(s)\ H_{\mathrm{ext}}(s)}{1 - \beta^T\ Y\ Z_L\ G(s)\ H_{\mathrm{ext}}(s)}. \tag{40}$$

III. Stability Analysis

To study the stability of the MSVC architecture, a Monte-Carlo analysis is conducted on MATLAB. The values of $|v_o|$,$|v_s|$, pf, and C_{dc} in (40) are randomly generated. The pole and zero locations and the phase margin of the system are calculated under different combinations of the intrinsic and extrinsic parameters, including supply voltage, loading condition, and dc-link capacitance. The ranges of the generated values are shown in Table II and the total number of samples used in each simulation is 5000. Assuming that their values are Gaussian distributed. Figs. 8–10 show the locations of the closed-loop system poles and zeros of the MSVC with three, two and one parallel-connected unit(s), respectively. It can be observed that all the poles and zeros lie on the left half *s*-plane. Fig. 11 shows the phase margin of MSVC with different ac mains voltages and different number of units engaged. The phase margin varies between 75° and 90° under the full-load condition, and between 40° and 90° under the 10% load condition. The results confirm the stability of the MSVC.

IV. Simplified Design Procedure

The design of the major power components is given in this section. The power components include $L_{q,r}$, $C_{q,r}$, and $C_{\mathrm{dc},r}$,

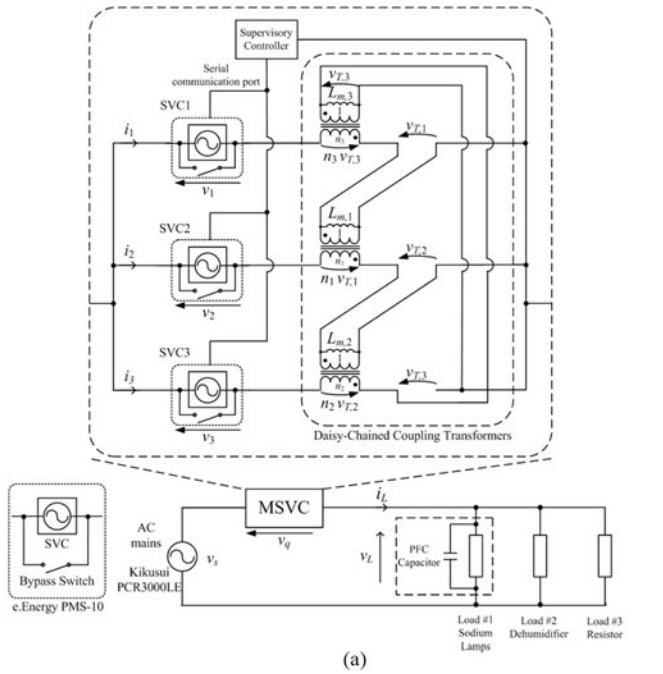

Fig. 13. Test setup. (a) Block diagram. (b) Photo.

and coupling transformers T_r. They are designed by using the parameters f_s, I_r, m, $\hat{v}_{\mathrm{dc},r}$, $v_{Lq,r}$, $\hat{i}_r$, f, and ω.

1) Step 1—Determination of the Voltage Rating of v_r.

The voltage rating of v_r is designed by considering that the resultant v_x meets the required compensation voltage even if $N-1$ of units are disengaged.

By substituting (9) and (13) into (7), the relationship between v and v_x is

$$v + KZY(\beta\, v_s - \ v) = \ \beta\, v_x. \tag{41}$$

Assuming that the all output voltage of engaged units are the same. Based on (41), the ratio between v_r and v_x is

$$\frac{v_r}{v_x} = \frac{N}{\text{Number of engaged units}}. \tag{42}$$

TABLE IV
LIST OF LOADS CONNECTED TO THE MSVC

Load	Description (Model)	Quantity	Rating (VA)	
			Inductive	Capacitive
#1	Sodium lamp (Philips SON-T Plus)	3	$460 \angle 29.5°$	$660 \angle -89°$
#2	Dehumidifier (Hitachi RD-2120E)	1	$550 \angle 29.5°$	
#3	Resistor	1	$1000 \angle 0°$	

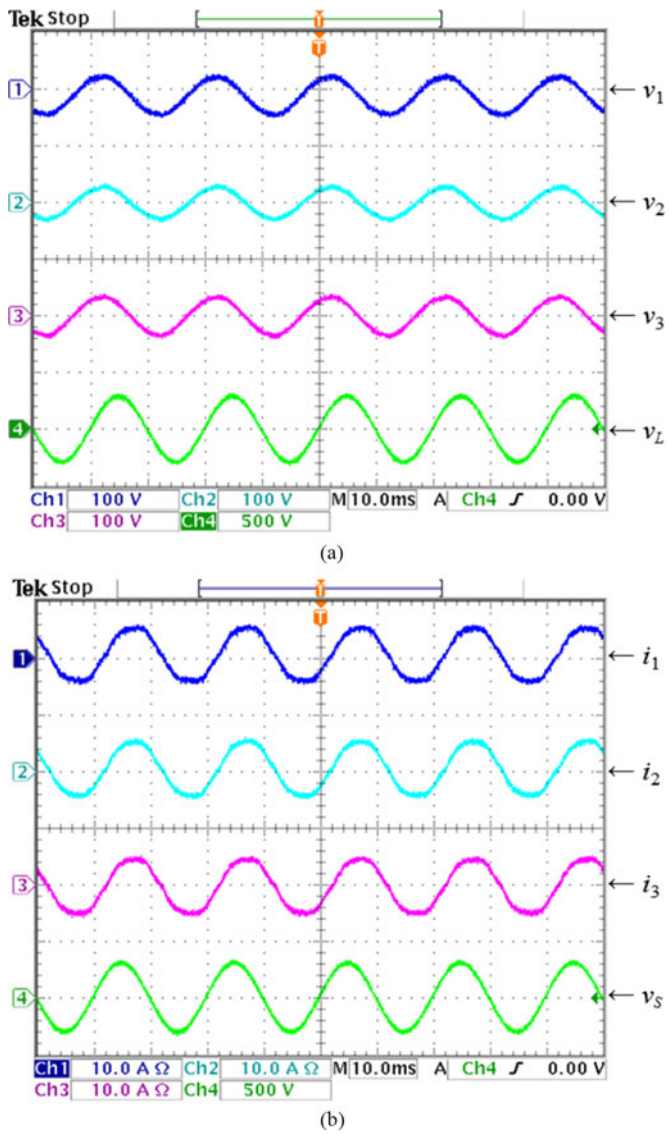

Fig. 14. Steady-state waveforms when the apparent power and power factor of the loads are 2745 VA and 0.82 (Timebase: 10 ms/div). (a) ν_1 (100 V/div), ν_2 (100 V/div), ν_3 (100 V/div) and ν_L (500 V/div). (b) i_1 (10 A/div), i_2 (10 A/div), i_3 (10 A/div) and ν_S (500 V/div).

By using (4), the required voltage rating of v_r can be determined.

2) Step 2—Determination of the Values of $L_{q,r}$, $C_{q,r}$, and $C_{\mathrm{dc},r}$.

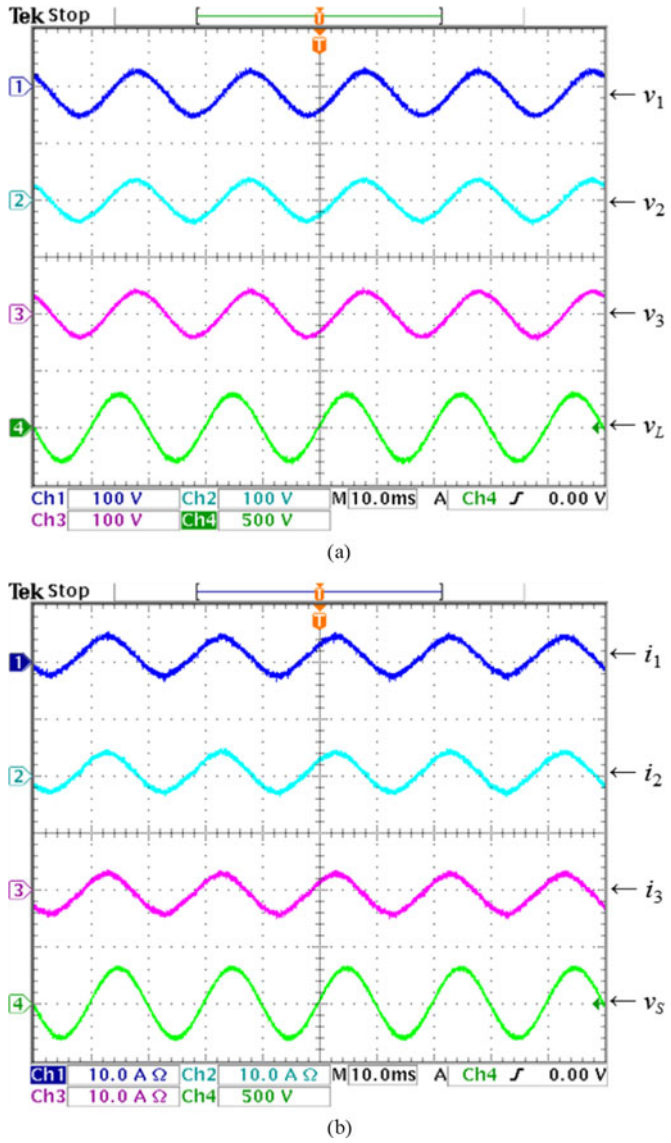

Fig. 15. Steady-state waveforms when the apparent power and the power factor of the loads are 1948 VA and −0.89 (Timebase: 10 ms/div). (a) ν_1 (100 V/div), ν_2 (100 V/div), ν_3 (100 V/div) and ν_L (500 V/div). (b) i_1 (10 A/div), i_2 (10 A/div), i_3 (10 A/div) and ν_S (500 V/div).

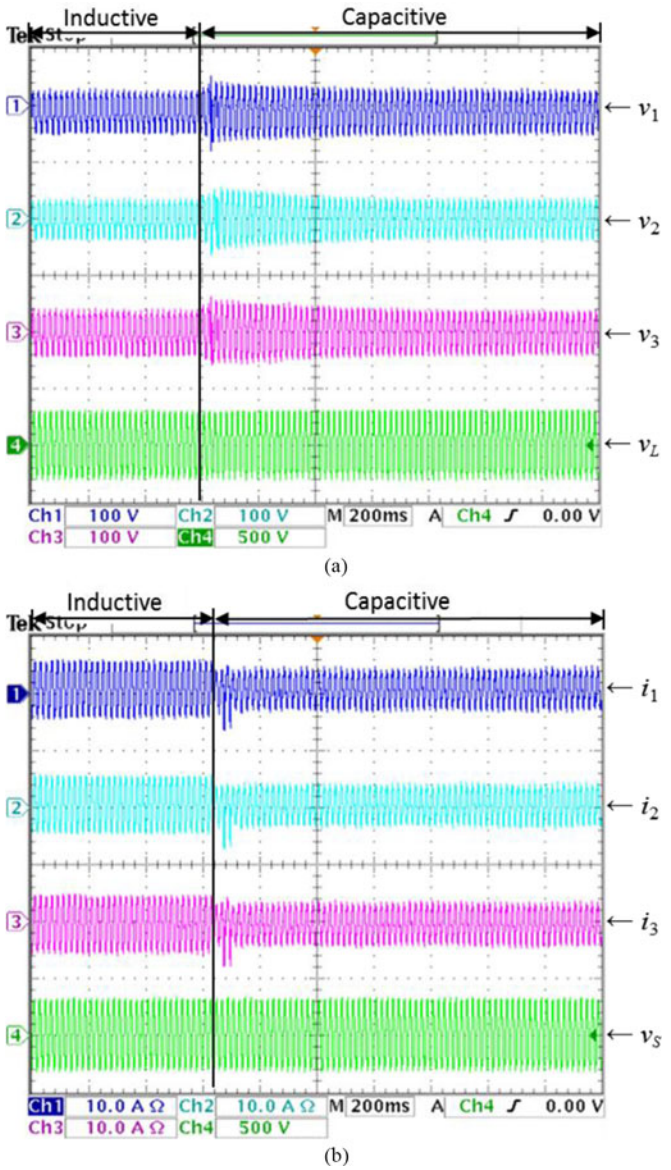

Fig. 16. Transient responses from the operation shown in Fig. 14 to the operation shown in Fig. 15 (Timebase: 200 ms/div). (a) ν_1 (100 V/div), ν_2 (100 V/div), ν_3 (100 V/div) and ν_L (500 V/div). (b) i_1 (10 A/div), i_2 (10 A/div), i_3 (10 A/div) and ν_S (500 V/div).

The values of $L_{q,r}$,$C_{q,r}$, and $C_{\mathrm{dc},r}$ are designed by using the method describing in [25] and [26]. That is

$$L_{q,r} \;<\; \frac{v_{Lq,r}}{2\,\pi\,f\,I_r} \tag{43}$$

$$C_{q,r} \;>\; \frac{1}{2\,\pi\,f_s\,(2\,\pi\,f_s\,L_{q,r} - \frac{4\,V_{\mathrm{dc}}}{\pi\,\hat{i}_r})} \tag{44}$$

and

$$C_{\mathrm{dc},r} \;=\; \frac{m}{8\,\omega}\;\frac{I_r}{\hat{v}_{\mathrm{dc},r}}. \tag{45}$$

3) Step 3—Design of T_r.

The maximum apparent power S_T of the transformer is

$$S_T \;=\; |v_{T,\max}\,|\,|i_{r,\max}\,| \tag{46}$$

where $|v_{T,\max}|$ and $|i_{r,\max}|$ are the maximum rms value of v_T and i_r, respectively.

Fig. 12 shows the $|v_{T,\max}|$ in terms of v_r for *N* varying from two to seven. A core geometry approach method is used to design the coupling transformer [27]. The core geometry, K_g, is

$$K_g = \frac{2S_T}{5.717\;f^2 B_m^2\;\sigma\;10^{-4}} \tag{47}$$

where B_m is the maximum flux density of the core and σ is the regulation of the transformer.

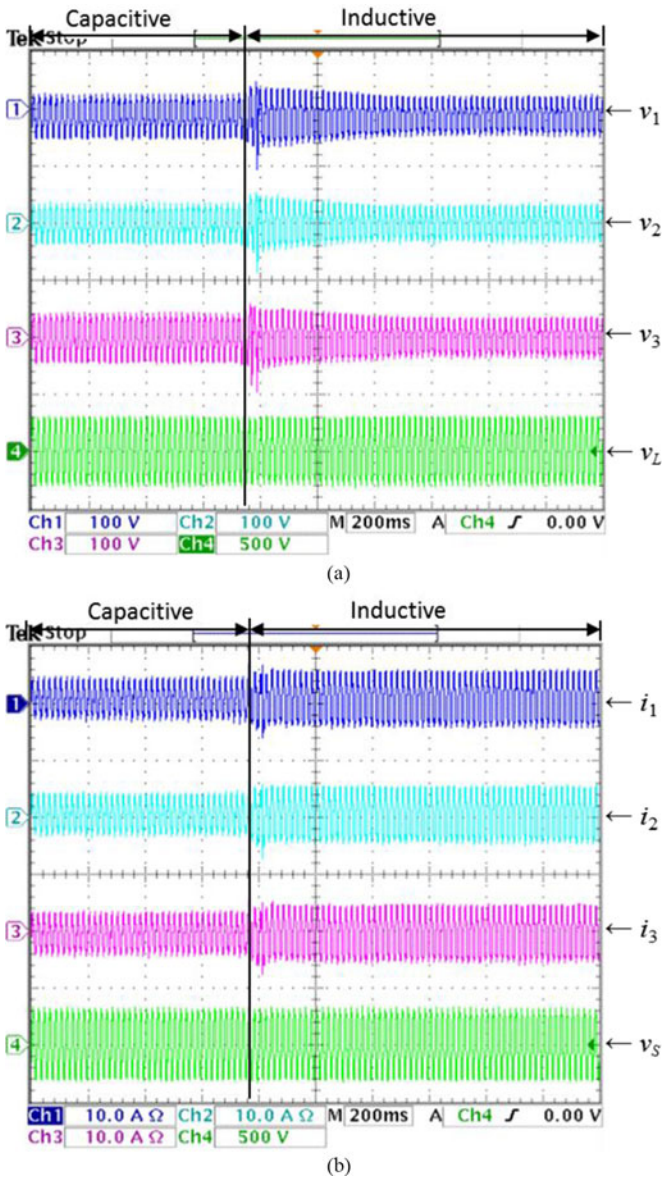

Fig. 17. Transient responses from the operation shown in Fig. 15 to the operation shown in Fig. 14 (Timebase: 200 ms/div). (a) ν_1 (100 V/div), ν_2 (100 V/div), ν_3 (100 V/div) and ν_L (500 V/div). (b) i_1 (10 A/div), i_2 (10 A/div), i_3 (10 A/div) and ν_S (500 V/div).

By applying the Faraday's Law, the number of turns N_p of the primary winding is determined by the formula given in [27]

$$N_p = \frac{|v_{T,\max}|(10^4)}{4.44A_c\ B_{\max}\ f}. \tag{48}$$

4) Step 4—Determinations of the Values of $K_{i,\text{ext}}$.

The values of K_p and K_i are determined by (30) for the given ξ_r and $\omega_{n,r}$. That is

$$K_i = \frac{\omega_{n,r}^2(\gamma_r B_r - A_r|i_r|\cos\theta_r)}{K_m\ (\gamma_r^2|i_r|^2 - 2\omega_{n,r}\xi_r\gamma_r|i_r|A_r + \omega_{n,r}^2A_r^2)} \tag{49}$$

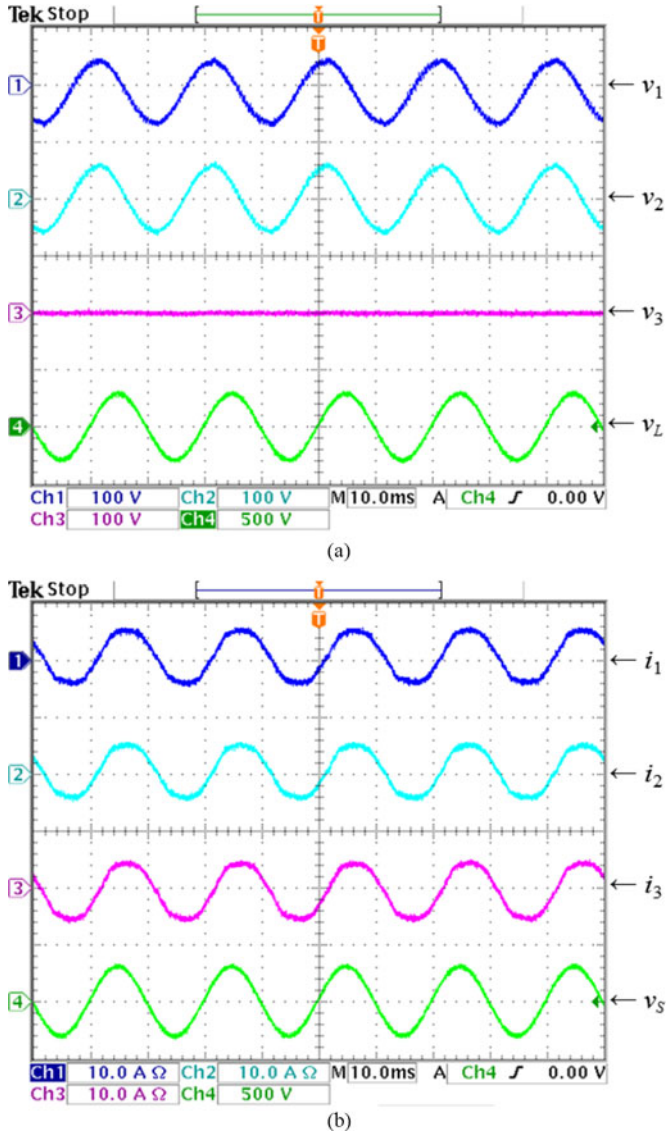

Fig. 18. Steady-state waveforms when one of the units is disengaged (Timebase: 10 ms/div). (a) ν_1 (100 V/div), ν_2 (100 V/div), ν_3 (100 V/div) and ν_L (500 V/div). (b) i_1 (10 A/div), i_2 (10 A/div), i_3 (10 A/div) and ν_S (500 V/div).

$$K_p = \frac{-\gamma_r|i_r|^2\cos\theta_r + 2\omega_{n,r}\xi_r\ \gamma_r B_r - \omega_{n,r}^2A_r^2\frac{1}{|v_r|\cos\theta_r}}{K_m\ (\gamma_r^2|i_r|^2 - 2\omega_{n,r}\xi_r\gamma_r A_r + \omega_{n,r}^2A_r^2)} \tag{50}$$

where $A_r = 4\ C_{\text{dc}}|v_{o,r}||v_r|\cos\theta_r$ and $B_r = 4\ C_{\text{dc},r}\ |i_r||v_{o,r}|$.

Typically, ξ_r is set to 0.7 and $\omega_{n,r}$ is set to five times of line cycle [28].

5) Step 5—Determinations of the Values of $K_{i,\text{ext}}$.

The value of $K_{i,\text{ext}}$ is determined by the time constant τ of the integrator. That is

$$K_{i,\text{ext}} = \frac{1}{\tau}. \tag{51}$$

In order to minimize the influence of each unit to the system response, τ is set to be five times slower than the natural frequency.

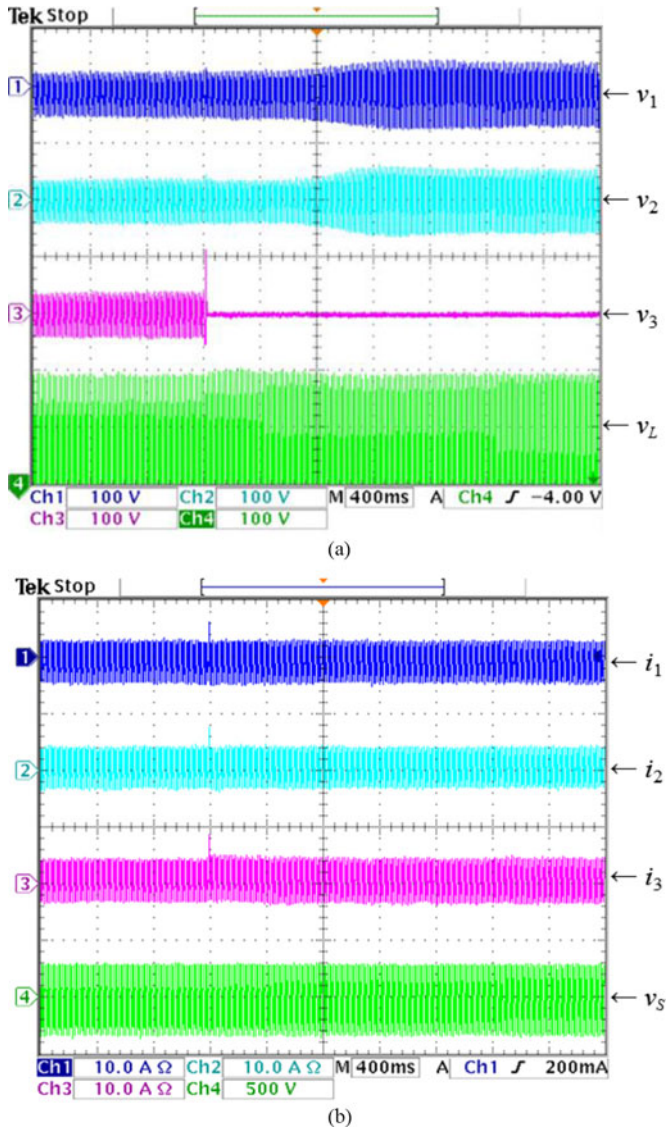

Fig. 19. Transient waveforms when one of the units is disengaged (Time-base: 400 ms/div). (a) ν_1 (100 V/div), ν_2 (100 V/div), ν_3 (100 V/div) and ν_L (500 V/div). (b) i_1 (10 A/div), i_2 (10 A/div), i_3 (10 A/div) and ν_S (500 V/div).

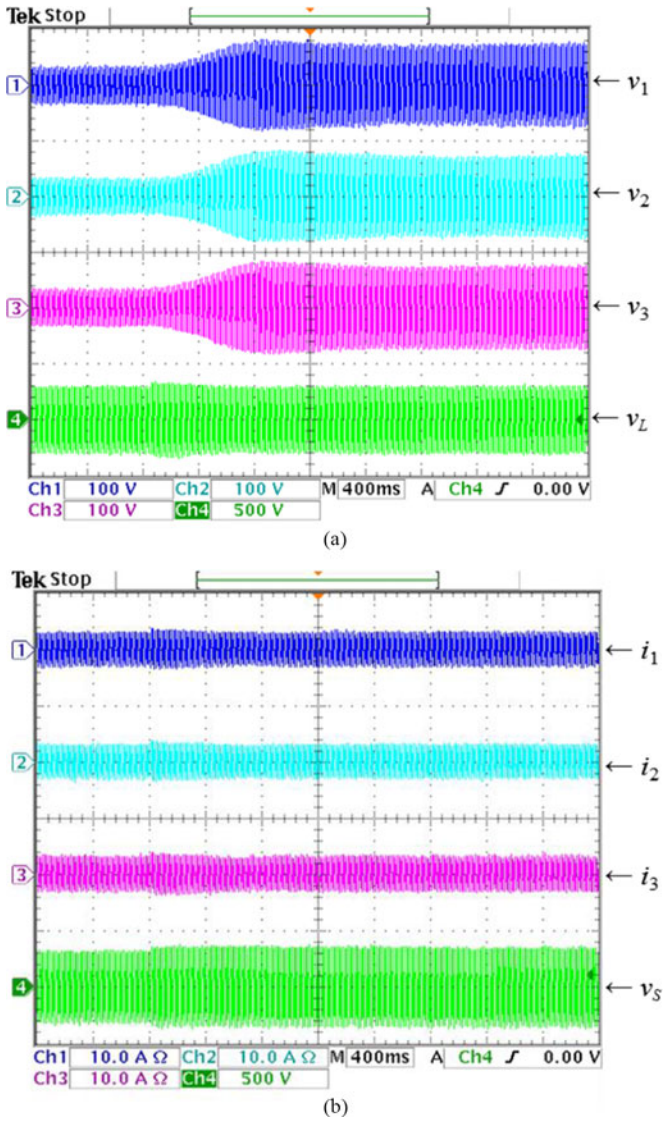

Fig. 20. Transient waveforms when $|v_s|$ change from 220 to 245 V (Time-base: 400 ms/div). (a) ν_1 (100 V/div), ν_2 (100 V/div), νv_3 (100 V/div) and ν_L (500 V/div). (b) i_1 (10 A/div), i_2 (10 A/div), i_3 (10 A/div) and ν_S (500 V/div).

V. Experimental Verifications

A 3-kVA, 220-V, 50-Hz prototype with three parallel-connected series voltage compensators has been built and evaluated. The design specification is given in Table III. Fig. 13 shows the testing setup, in which the MSVC is used to supply three sets of loads, including sodium lamps, dehumidifiers, and a resistor bank. The setup simulates a typical residential environment with varying load power and power factor. The power ratings of the loads are listed in Table IV. Each SVC unit has an internal bypass switch across its output. The switch will be closed when the unit is disengaged. A Freescale's digital signal processor is used for the supervisory controller. The three coupling transformers, T_1, T_2, and T_3, have the magnetizing inductances of 162, 152 and 160 mH, respectively. The reference voltage $v_{\mathrm{ref},r}$ and $v_{\mathrm{ref,ext}}$ are all set to 205 V.

When all the sodium lamps among the loads are in normal operation, its input is inductive. The apparent power and power factor of the loads are 2745 VA and 0.82. Fig. 14(a) shows the steady-state voltage waveforms of v_1, v_2, v_3, and v_L. Fig. 14(b) shows the steady-state waveforms of i_1, i_2, $i_3$and v_S. The current through all compensators is 3.5 A. When the lamp goes off and the PFC capacitor is still connected across the input of the lamp ballast, its input becomes capacitive. The apparent power and power factor of the loads are 1948 VA and –0.89. Fig. 15(a) shows the steady-state voltage waveforms of v_1, v_2, v_3, and v_L. Fig. 15(b) shows the steady-state waveforms of i_1, i_2, $i_3$and v_S. The current through all compensators is 2.3 A. The voltage and current waveforms of the three units are similar in the above test, confirming the operation of MSVC.

Fig. 16 shows the transient waveforms when the system is changed from the operation shown in Fig. 14 into the operation

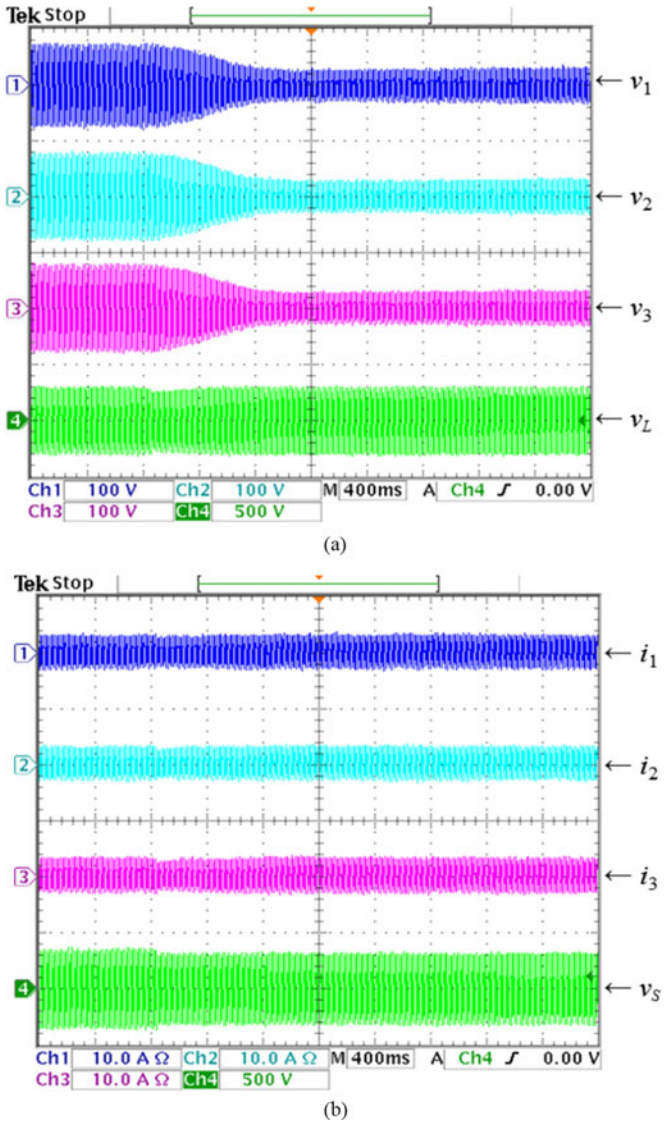

Fig. 21. Transient waveforms when $|v_s|$ change from 245 to 220 V (Timebase: 400 ms/div). (a) ν_1 (100 V/div), ν_2 (100 V/div), ν_3 (100 V/div) and ν_L (500 V/div). (b) i_1 (10 A/div), i_2 (10 A/div), i_3 (10 A/div) and ν_S (500 V/div).

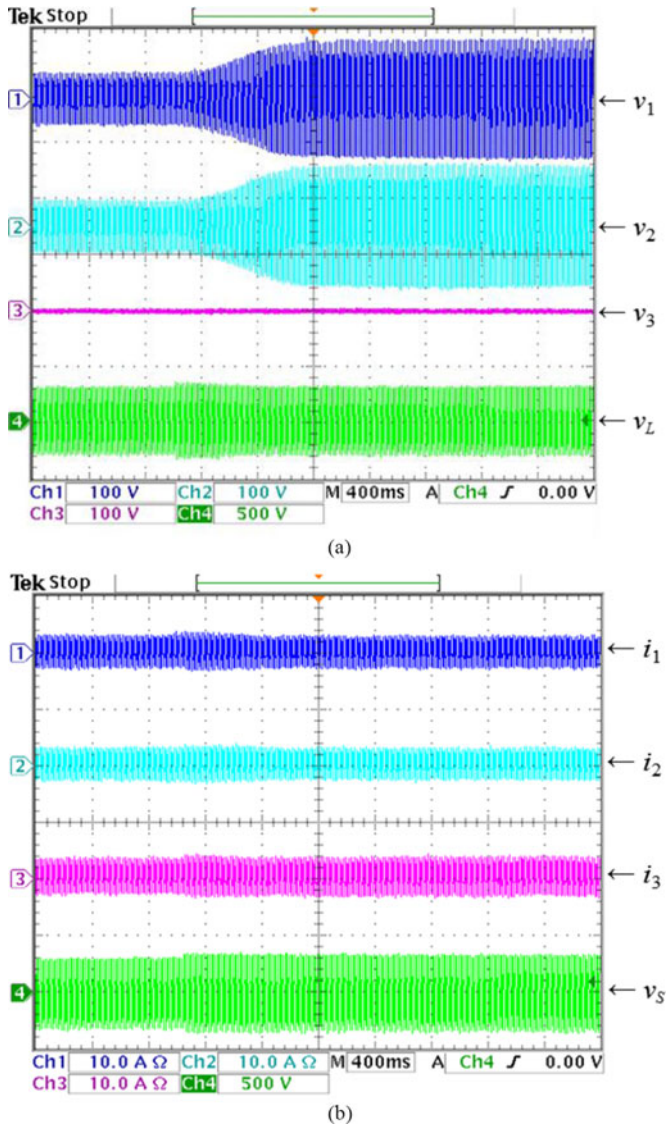

Fig. 22. Transient waveforms when $|v_s|$ change from 220 to 245 V and one of the units is disengaged (Timebase: 400 ms/div). (a) ν_1 (100 V/div), ν_2 (100 V/div), ν_3 (100 V/div) and v_L (500 V/div). (b) i_1 (10 A/div), i_2 (10 A/div), i_3 (10 A/div) and ν_S (500 V/div).

shown in Fig. 15. Fig. 17 shows the transient waveforms when the system is changed from the operation shown in Fig. 15 into the operation shown in Fig. 14. It can be observed that the voltage and current waveforms of the three units are similar, confirming the proposed method of current sharing among the units.

Figs. 18 and 19 show the steady-state waveforms and transient waveforms, respectively, when one of the compensators is disengaged from the system. The three currents are shared equally, due to the daisy-chained transformers. The results shown that the voltage supplying to the loads can still be regulated at 205 V, confirming the function of supervisory control and the service continuity of the proposed MSVC structure.

Figs. 20 and 21 show the transient waveforms when $|v_s|$ is changed from 220 to 245 V and from 245 to 220 V, respectively. Fig. 22 shows the transient waveforms when $|v_s|$ is changed from 220 to 245 V and one of the units is disengaged. Fig. 23 shows the transient waveforms when $|v_s|$ is changed from 245 to 220 V and one of the units is disengaged. The three currents are almost the same even under voltage transient. The results show that the voltage supplying to the loads can still be regulated at 205 V, confirming the voltage disturbance rejection ability of the system and the service continuity of the proposed MSVC structure. The experimental results also confirm the stability of the global system, as discussed in Section III.

VI. Conclusion

The concept of the MSVC architecture has been presented in this paper. It can enhance the service continuity and flexibly increase the power rating of voltage regulator in power systems, and has an advantage of high modularity, scalability

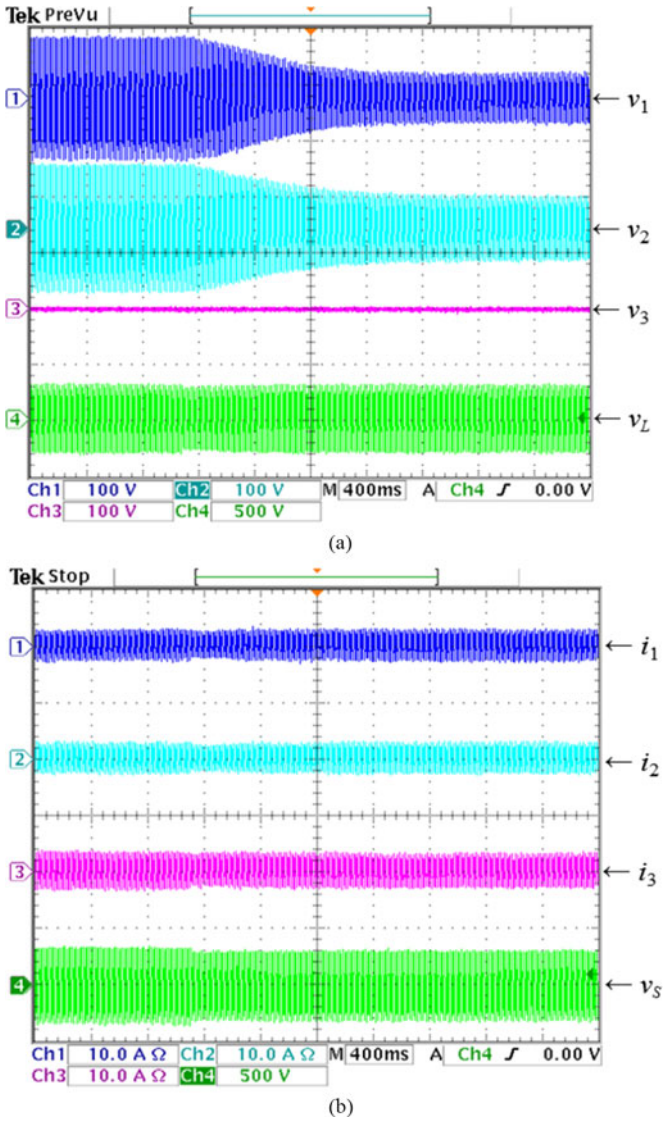

Fig. 23. Transient waveforms when $|v_s|$ change from 245 to 220 V and one of the units is disengaged (Timebase: 400 ms/div). (a) ν_1 (100 V/div), ν_2 (100 V/div), ν_3 (100 V/div) and ν_L (500 V/div). (b) i_1 (10 A/div), i_2 (10 A/div), i_3 (10 A/div) and ν_S (500 V/div).

and adaptability. Detailed mathematical treatments and modeling have been presented. The stability of the MSVC system with different number of engaged units and under wide parametric variations is also confirmed by conducting Monte-Carlo analyses on MATLAB. A 3-kVA series voltage regulator test bed with the MSVC concept has been built and evaluated. The system has also adopted a supervisory control. The experimental results show that the load current is shared among each unit equally and the load voltage is tightly regulated.

APPENDIX

A. Derivations of (2) and (3)

By applying the Kirchhoff's current law

$$i_L = \frac{|v_s|}{|Z_L|}\angle(-\theta) - \frac{|v_x|}{|Z_L|}\angle(\phi_x - \theta). \tag{A.1}$$

The apparent power S_x handled by the MSVC is

$$S_x = v_x\, i_L^* = \frac{|v_x|\,|v_s|}{|Z_L|}\angle(\phi_x + \theta) - \frac{|v_x|^2}{|Z_L|}\angle\theta \tag{A.2}$$

where i_L^* is the conjugate of i_L.

Thus

$$P_x = \frac{|v_x|\,|v_s|}{|Z_L|}\cos(\phi_x + \theta) - \frac{|v_x|^2}{|Z_L|}\cos\theta \tag{2}$$

$$Q_x = \frac{|v_x|\,|v_s|}{|Z_L|}\sin(\phi_x + \theta) - \frac{|v_x|^2}{|Z_L|}\sin\theta. \tag{3}$$

B. Proof of (4) and (5)

Based on Fig. 2, by applying the Pythagoras's theorem and the sine rule

$$|v_s|^2 = [|v_L|\cos(\alpha\theta)]^2 + [|v_x| + |v_L|\sin(\alpha\theta)]^2$$
$$|v_x| = \sqrt{|v_s|^2 - (|v_L|\cos\theta)^2} - |v_L|\sin(\alpha\theta) \text{ for Case I} \tag{A.3}$$

and

$$|v_s|^2 = [|v_L|\cos(\alpha\theta)]^2 + [-|v_x| + |v_L|\sin(\alpha\theta)]^2$$
$$|v_x| = -\sqrt{|v_s|^2 - (|v_L|\cos\theta)^2} + |v_L|\sin(\alpha\theta) \text{ for Case II.} \tag{A.4}$$

By generalizing (A.3) and (A.4)

$$|v_x| = K_L[\sqrt{|v_s|^2 - (|v_L|\cos\theta)^2} - |v_L|\sin(\alpha\theta)]. \tag{4}$$

Based on Fig. 2, after applying the sine rule

$$\frac{|v_L|}{\sin(\alpha\phi_x)} = \frac{|v_s|}{\sin(90^o + \alpha\theta)}$$
$$\phi_x = \alpha\sin^{-1}\left(\frac{|v_L|\cos\theta}{|v_s|}\right) \text{ for Case I} \tag{A.5}$$

and

$$\frac{|v_L|}{\sin(-\alpha\phi_x)} = \frac{|v_s|}{\sin(90^o - \alpha\theta)}$$
$$\phi_x = -\alpha\sin^{-1}\left(\frac{|v_L|\cos\theta}{|v_s|}\right) \text{ for Case II.} \tag{A.6}$$

By generalizing (A.5) and (A.6)

$$\phi_x = K_L\alpha\sin^{-1}\left(\frac{|v_L|\cos\theta}{|v_s|}\right). \tag{5}$$

ACKNOWLEDGMENT

The authors would like to thank e.Energy Lighting Limited for the technical support for building the experimental prototypes.

REFERENCES

[1] G. Joos, B. T. Ooi, D. McGillis, F. D. Galiana, and R. Marceau, "The potential of distributed generation to provide ancillary services," in *Proc. IEEE Power Eng. Soc. Summer Meeting*, 2000, pp. 1762–1767.

[2] G. T. Heydt, "The next generation of power distribution systems," *IEEE Trans. Smart Grid*, vol. 1, no. 3, pp. 225–235, Dec. 2010.

[3] O. P. Mccarty, "Transformer voltage regulator," U.S. Patent 2 063 693 S, Dec. 8, 1936.
[4] R. L. Hirschfeld, "Power control unit for automatic control of power consumption in a lighting load," U.S. Patent 4 189 664, Feb. 19, 1980.
[5] M. H. Lee, "Automatic voltage regulator," U.S. Patent 8 415 934 B2, Apr. 9, 2013.
[6] M. H. Hedayati, A. B. Acharya, and V. John, "Common-mode filter design for PWM rectifier-based motor drives," *IEEE Trans. Power Electron.*, vol. 28, no. 11, pp. 5364–5371, Nov. 2013.
[7] P. Mlodzikowski, A. Milczarek, S. Stynski, M. Malinowski, and S. Kouro, "Control of simplified multilevel AC-DC-AC converter for small power generation systems," in *Proc. Ind. Electron. Soc.*, 2013, pp. 5951–5956.
[8] Y. Li, L. Shi, and H. Zhang, "Real-time simulation of linear synchronous motor drives with AC-DC-AC converters," in *Proc. IEEE Conf. Ind. Electron. Appl.*, 2011, pp. 680–685.
[9] N. H. Woodley, L. Morgan, and A. Sundaram, "Experience with an inverter-based dynamics voltage restorer," *IEEE Trans. Power Del.*, vol. 14, no. 3, pp. 1181–1186, Jul. 1999.
[10] A. Campos, G. Jobs, P. D. Ziogas, and J. F. Lindsay, "Analysis and design of a series-connected PWM voltage regulator for single-phase AC sources," *IEEE Trans. Ind. Appl.*, vol. 32, no. 6, pp. 1285–1292, Nov./Dec. 1996.
[11] P. Kumar and K. Namrata, "Voltage control and power oscillation damping of multi-area power system using static synchronous series compensator," *IOSR J. Electr. Electron. Eng.*, vol. 1, no. 5, pp. 26–33, 2012.
[12] S. Dasgupta, S. Sahoo, S. Panda, and G. A. J. Amaratunga, "Single-phase inverter control techniques for interfacing renewable energy sources with micro-grid—Part II: Series connected inverter topology to mitigate voltage related problems along with active power flow control," *IEEE Trans. Power Electron.*, vol. 26, no. 3, pp. 732–746, Mar. 2011
[13] S. Zhang, K.-J. Tseng, S. S. Choi, T. D. Nguyen, and D. L. Yao, "Advanced control of series voltage compensation to enhance wind turbine ride through," *IEEE Trans. Power Electron.*, vol. 27, no. 2, pp. 763–772, Feb. 2012.
[14] V. Cheung, H. Chung, and A. Lo, "Phase jump technique for minimization of load voltage transients in SSSC-based voltage regulator," in *Proc. IEEE Appl. Power Electron. Conf.*, 2014, pp. 1205–1212.
[15] J. Chen and C. Chu, "Combination voltage-controlled and current-controlled PWM inverters for UPS parallel operation," *IEEE Trans. Power Electron.*, vol. 10, no. 5, pp. 547–558, Sep. 1995.
[16] Y. Q. Pei, G. B. Jiang, Y. Xu, and Z. A. Wang, "Auto-master-slave control technique of parallel inverters in distributed AC power systems and UPS," in *Proc. IEEE 35th Power Electron. Spec. Conf.*, 2004, pp. 2050–2053.
[17] A. P. Martins, A. S. Carvalho, and A. S. Araújo, "Design and implementation of a current controller for the parallel operation of standard UPSs," in *Proc. IEEE 21st Int. Conf. Ind. Electron.*, 1995, pp. 584–589.
[18] M. Borrega, L. Marroyo, R. Gonzalez, J. Balda, and J. Agorreta, "Modeling and control of a master-slave PV inverter with N-paralleled inverters and three-phase three-limb inductors," *IEEE Trans. Power Electron.*, vol. 28, no. 6, pp. 2842–2855, Jun. 2013.
[19] T. Iwade, S. Komiyama, and Y. Tanimura, "A novel small-scale UPS using a parallel redundant operation system," in *Proc. IEEE 25th Int. Telecommun. Energy Conf.*, 2003, pp. 480–483.
[20] X. Sun, L. K. Wong, Y. S. Lee, and D. H. Xu, "Design and analysis of an optimal controller for parallel multi-inverter systems," *IEEE Trans. Circuits Syst. II: Exp. Briefs*, vol. 53, no. 1, pp. 56–61, Jan. 2006.
[21] L. Corradini, P.Mattavelli, M. Corradin, and F. Polo, "Analysis of parallel operation of uninterruptible power supplies loaded through long wiring cables," *IEEE Trans. Power Electron.*, vol. 25, no. 4, pp. 1046–1054, Apr. 2010.
[22] Y. K. Chen, T. F. Wu, Y. E. Wu, and C. P. Ku, "A current-sharing control strategy for paralleled multi-inverter systems using microprocessor-based robust control," in *Proc. IEEE 10th Int. Electr. Electron. Technol. Conf.*, 2001, pp. 647–653.
[23] X. Sun, Y. S. Lee, and D. Xu, "Modeling, analysis, and implementation of parallel multi-inverter system with instantaneous average-current-sharing scheme," *IEEE Trans. Power Electron.*, vol. 18, no. 3, pp. 844–856, May 2003.
[24] A. M. Roslan, K. H. Ahmed, S. J. Finney, and B. W. Williams, "Improved instantaneous average current sharing control scheme for parallel connected inverter considering line impedance impact in microgrid networks," *IEEE Trans. Power Electron.*, vol. 26, no. 3, pp. 702–716, Mar. 2011.
[25] V. Cheung, H. Chung, K. Wang, and A. Lo, "Paralleling multiple static synchronous series compensators using daisy-chained transformers," *IEEE Trans. Power Electron.*, vol. 29, no. 6, pp. 2764–2773, Jun. 2014.
[26] C. Ho and H. Chung, "Implementation and performance evaluation of a fast dynamic control scheme for capacitor-supported interline DVR," *IEEE Trans. Power Electron.*, vol. 25, no. 8, pp. 1975–1988, Aug. 2010.
[27] C. W. T. McLyman, *Transformer and Inductor Design Handbook*. Boca Raton, FL, USA: CRC Press, 2011.
[28] K. Ogata, *Modern Control Engineering*. Englewood Cliffs, NJ, USA: Prentice Hall, 2002.

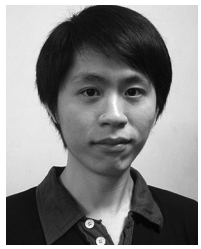

Victor Sui-Pung Cheung received the B.Eng. degree in electronic and communication engineering in 2008 from the City University of Hong Kong, Hong Kong, where he is currently working toward the M.Phil. degree.

Since 2008, he has been a Research Assistant at the Centre for Smart Energy Conversion and Utilization Research, City University of Hong Kong. His research interests include grid-connected inverter, reactive power compensation, modeling and control of power converters.

Henry Shu-hung Chung (M'95–SM'03) received the B.Eng. degree in 1991 and the Ph.D. degree in 1994 in electrical engineering, both from the Hong Kong Polytechnic University, Hong Kong.

Since 1995, he has been with the City University of Hong Kong, Hong Kong. He is currently Professor at the Department of Electronic Engineering, and the Director of the Centre for Smart Energy Conversion and Utilization Research. His research interests include time- and frequency-domain analysis of power electronic circuits, switched-capacitor-based converters, random-switching techniques, control methods, digital audio amplifiers, soft-switching converters, and electronic ballast design. He has edited one book, and authored eight research book chapters, and more than 320 technical papers including 160 refereed journal papers in his research areas, and holds 34 patents.

Dr. Chung is currently Editor-in-Chief of the IEEE POWER ELECTRONICS LETTERS, and Associate Editor of the IEEE TRANSACTIONS ON POWER ELECTRONICS, and IEEE JOURNAL OF EMERGING AND SELECTED TOPICS IN POWER ELECTRONICS.

Alan Wai-Lun Lo (M'02) received the B.Eng. degree in electrical engineering and the Ph.D. degree from the Hong Kong Polytechnic University, Hong Kong, in 1991 and 1996, respectively.

He has been a Research Assistant and then a Research Associate at the Department of Electrical Engineering, Hong Kong Polytechnic University, from 1996 to 1997. From 1997 to 1999, he was a Postdoctoral Fellow at the Department of Electrical Engineering, Hong Kong Polytechnic University. In 1999, he was with the Department of Electronic Engineering, City University of Hong Kong, Hong Kong, as a Research Fellow before joining the Department of Computer Science, Chu Hai College of Higher Education, Hong Kong, in September 1999. He is currently the Head of the Department of Computer Science, Chu Hai College of Higher Education. He is currently an Advisor for the Centre of the Power Electronic, City University of Hong Kong. His research interest includes adaptive control, fuzzy control, intelligent control via neural network and applications of genetic algorithm.